

OVERVIEW OF CRITICAL ISSUES AND OPPORTUNITIES FOR NEW A/C WITH HYBRID AND FULL-ELECTRIC POWERTRAIN

Fabrizio Nicolosi[1], Mario Di Stasio[1]

[1]University of Naples Federico II (UNINA), Department of Industrial Engineering, DAF research group

Abstract

This paper investigates the aircraft-level impact of technology-related assumptions for advanced regional aircraft with electric and hybrid-electric powertrains. Two conceptual design studies are performed: a 100-passenger liquid-hydrogen fuel-cell aircraft and an 80-passenger battery-based parallel hybrid-electric aircraft coupled with gas turbines. For the fuel-cell configuration, fuel-cell efficiency, specific power, balance-of-plant characteristics, hydrogen-tank gravimetric index, and cooling-related aerodynamic penalties are varied to quantify their effect on optimized aircraft sizing and mission hydrogen consumption. For the hybrid-electric configuration, battery gravimetric energy density, installed battery energy, hybridization factor, and shaft power are assessed against fixed TLARs. Results show that fuel-cell aircraft are particularly sensitive to cooling-drag recovery and fuel-cell efficiency, while battery-based hybrid-electric benefits are strongly constrained by battery mass. The study highlights the need for aircraft-level assessment of emerging propulsion technologies beyond component-level indicators.

Keywords: aircraft, conceptual design, hybrid-electric propulsion system, hydrogen

1. Context and objectives

Aviation decarbonization is driving increasing interest in propulsion architectures that depart substantially from conventional kerosene-fuelled thermal engines. Among the most investigated options for short- and medium-range applications are battery-electric, hybrid-electric, and hydrogen fuel-cell-based powertrains, in which electric motor drives, power electronics, batteries, fuel cells, and cryogenic hydrogen storage may partially or fully replace conventional gas-turbine or piston-engine systems. Regional and short-range propeller-driven aircraft represent a particularly relevant application domain for these technologies, since their moderate payload-range requirements are more compatible with the present and projected limitations of electric and hydrogen-based propulsion systems [1][2][3].

However, the aircraft-level feasibility of these architectures strongly depends on technology-related key performance indicators whose future values remain uncertain. For hydrogen fuel-cell aircraft, relevant assumptions include fuel-cell efficiency, system-level specific power, balance-of-plant mass, liquid-hydrogen (LH2) tank gravimetric index, fuel supply installation, and the mass and drag penalties associated with thermal management. For battery-based hybrid-electric aircraft, the achievable benefits are instead closely linked to battery gravimetric energy density, installed battery capacity, and degree of hybridization of the propulsion system. Since these parameters directly affect aircraft mass, installed power, aerodynamic characteristics, energy demand, and compliance with top-level aircraft requirements (TLARs), their impact cannot be assessed only at component level.

Several recent studies have investigated hydrogen fuel-cell [4][5][6][7][8] and battery-based hybrid-electric propulsion [9][10] for regional aircraft, highlighting their potential for fuel-burn and emission reduction, but also the severe penalties associated with propulsion-system mass, energy storage, payload capability, and thermal management. Nevertheless, many conceptual design studies are based on a fixed set of technology assumptions, which may obscure the sensitivity of the final aircraft design to the assumed maturity level of the underlying powerplant technologies. A systematic aircraft-level assessment is therefore required to quantify how variations in these assumptions

propagate to aircraft sizing, performance, and potential operational benefits.

This work addresses this need through two complementary conceptual design studies on regional propeller-driven aircraft. The first analysis investigates a full-electric architecture based on liquid-hydrogen-fed fuel cells for a 100-passenger regional aircraft, focusing on the impact of fuel-cell and hydrogen-storage technology assumptions on the resulting aircraft configuration. The second analysis considers an 80-passenger, 800-nm-class regional aircraft equipped with a parallel hybrid-electric powerplant, and evaluates the combined influence of battery energy density, degree of hybridization, installed battery capacity, and total shaft power on aircraft performance, top-level requirement compliance, and fuel-saving potential.

2. Implementation

2.1 JPAD-based conceptual design framework

The aircraft-level analyses presented in this work are carried out using JPAD, a modular conceptual and preliminary aircraft design framework developed at the University of Naples Federico II by the DAF research group, in collaboration with SmartUp Engineering [11][12][13]. The framework builds on the experience gained by the research group in multidisciplinary aircraft design and optimization activities, including collaborative design studies performed within previous European research projects [14][15][16]. JPAD is based on an object-oriented architecture implemented in Java and provides an integrated environment for the parametric definition, sizing, and performance assessment of conventional and unconventional aircraft configurations.

Within JPAD, the aircraft is described through a hierarchical set of geometrical, aerodynamic, structural, systems, and propulsion-related parameters. This allows the main aircraft characteristics to be automatically updated when design variables or technology assumptions are modified. The framework supports the evaluation of mass breakdown, centre-of-gravity position, aerodynamic characteristics, stability-relevant quantities, and mission performance. Flight performance is evaluated through simulation-based routines, including time-marching methods and, when required, the solution of systems of ordinary differential equations for mission analysis.

A central feature for the present work is the capability of JPAD to model different propulsion architectures within a common aircraft sizing environment. The powerplant is represented through a modular component-based approach, in which the main elements of the propulsion chain are described separately and then integrated at aircraft level. Depending on the considered configuration, these components may include conventional thermal engines, fuel cells, batteries, electric machines, converters, inverters, gearboxes, propellers, auxiliary systems, and energy storage subsystems. This structure makes it possible to propagate technology-related assumptions from component level to aircraft level, evaluating their impact on installed mass, occupied volume, available shaft power, propulsion-chain efficiency, mission energy demand, fuel or hydrogen consumption, and aircraft-level requirement compliance.

For all the electric and hybrid-electric architectures considered in this paper, the propulsion system is modelled using a bottom-up approach. In the case of hydrogen fuel-cell configurations, the modelling starts from fuel-cell-system assumptions, such as efficiency, system-level specific power, auxiliary loads, and balance-of-plant contributions. These parameters are used to estimate the installed fuel-cell-system mass, the available electric power, and the hydrogen consumption associated with the mission power profile. The electric power generated by the fuel cells is then propagated through the downstream components of the propulsion chain, including power electronics, electric machines, and reduction gearboxes, so that the effective shaft power available to the aircraft can be evaluated during the different flight phases.

An analogous bottom-up strategy is adopted for battery-based electric and hybrid-electric configurations. In this case, the modelling starts from battery-cell characteristics and proceeds towards the definition of the battery module and battery pack. Given the required pack voltage, total battery capacity, and expected output power, JPAD estimates the number of cells and modules required and their arrangement in series and parallel connections. This simplified pack-level representation allows the main battery mass and volume requirements to be assessed, supporting a preliminary allocation of battery installation space within the aircraft. The battery system is then

integrated with the electric branch of the propulsion architecture, accounting for losses associated with converters, inverters, electric machines, and reduction gearboxes along the power transmission chain. For hybrid-electric configurations, the conventional thermal engine provides part of the required shaft power and is associated with fuel consumption according to the selected engine performance model, while the electric branch supplies the remaining contribution according to the prescribed degree of hybridization and installed battery capacity. The sum of the thermal and electric contributions defines the total available shaft power.

For the liquid-hydrogen case, the sizing of the cryogenic hydrogen storage system is performed through a MATLAB-based tool derived from the methodology proposed by Winnefeld et al. [17]. The tool estimates tank geometry, structural mass, insulation mass, and overall storage-system characteristics as a function of the required hydrogen mass, mission profile, dormancy requirement, venting pressure, and installation constraints. The resulting tank size and mass are then passed back to the aircraft design loop, so that the aircraft geometry and mass breakdown remain consistent with the required hydrogen storage volume.

The overall workflow adopted for the hydrogen-powered full-electric configuration is shown in Figure 1. The process starts from the definition of a baseline aircraft, a set of top-level aircraft requirements, and a set of technology-level assumptions for both the airframe and the powerplant. The selected design variables, such as wing planform characteristics and installed power, are used to update the aircraft geometry and the corresponding derived quantities, including wing span, fuselage dimensions, tailplane layout, nacelle arrangement, propulsion-system installation, and onboard systems positioning. The updated aircraft is then analysed through coupled convergence loops. A first loop ensures consistency among aircraft mass, mission hydrogen consumption, and maximum take-off mass. A second loop addresses the integration of the liquid-hydrogen storage system, by checking the compatibility between the required hydrogen mass, the resulting tank size, and the available installation volume. Once convergence is reached, the final configuration is assessed in terms of complete flight performance and requirement compliance.

A simpler, JPAD-based workflow is adopted for the battery-based parallel hybrid-electric configuration. In this case, the aircraft sizing process remains closer to the conventional turboprop design loop, since no cryogenic storage volume convergence is required. The main additional modelling elements concern the definition of the hybrid-electric powerplant, including the split between thermal and electric shaft power, the installed battery energy, the battery gravimetric energy density, and the battery pack arrangement. For each combination of technology assumptions and hybridization level, JPAD evaluates the resulting aircraft mass, installed power, mission fuel consumption, and battery energy usage. The design loop is therefore essentially driven by the convergence between design mission fuel mass, battery mass, and maximum take-off mass.

The converged aircraft designs obtained from both workflows are finally used to build response surfaces and design-space representations. These response surfaces allow the sensitivity of the final aircraft configuration to the selected technology assumptions to be quantified, and make it possible to identify feasible combinations of design variables and powerplant technology levels. Optimization studies are then performed by selecting the configurations that satisfy all imposed top-level aircraft requirements while minimizing the selected aircraft-level objective, such as mission fuel consumption or total mission energy demand.

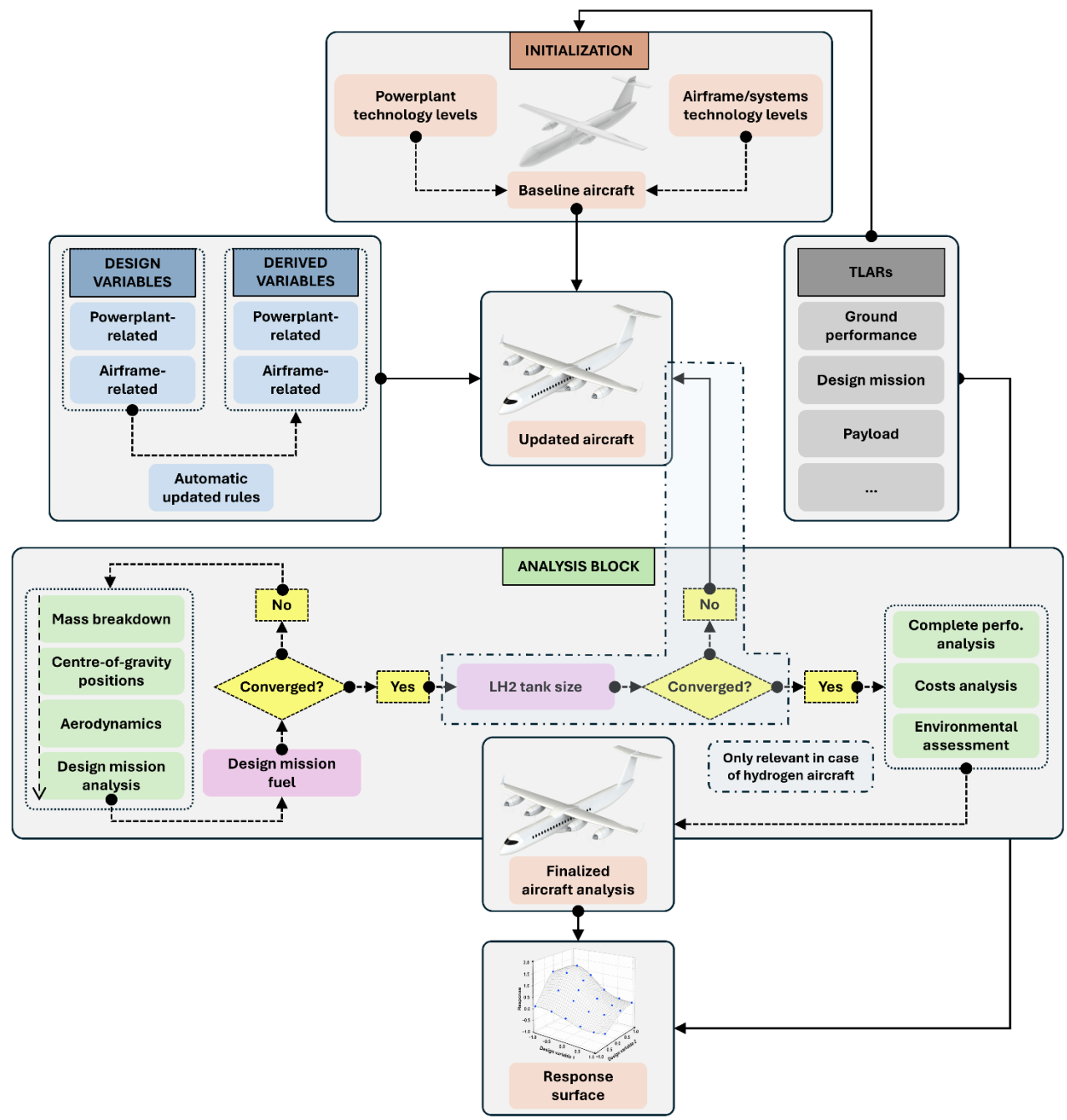


Figure 1 – General JPAD-based conceptual design workflow. The process includes the initialization of technology-level assumptions, the selection of aircraft design variables, iterative convergence on masses, and the generation of response surfaces for aircraft-level sensitivity and optimization studies. A hydrogen tank sizing loop is activated only for hydrogen-powered configurations with fuselage-mounted storage system.

2.2 Technology-level assumptions and parametric investigation

The two aircraft-level studies presented in this work rely on different sets of technology assumptions, reflecting the different expected maturity levels of the considered propulsion architectures. The hydrogen fuel-cell configuration is assumed to target an entry into service (EIS) around 2040, when fuel-cell propulsion systems for aviation are expected to reach a higher level of technological maturity. Conversely, the battery-based hybrid-electric configuration is considered closer to a 2030 EIS horizon and is therefore based on more conservative assumptions, without introducing additional structural or aerodynamic improvements with respect to state-of-the-art regional turboprop aircraft.

All the aircraft configurations examined in the paper adopt the same cabin arrangement, based on a 2+3 abreast layout. However, the two studies differ in terms of propulsion architecture, design strategy, number of propulsive units, and assumed airframe technology level, as described in the

following subsections.

2.2.1 Hydrogen fuel-cell full-electric configuration

The first aircraft-level analysis focuses on a full-electric regional aircraft powered by liquid-hydrogen fuel-cell systems. The configuration adopts a four-engine layout, with the propulsive units installed on the wing and supplied by two cryogenic hydrogen tanks arranged in tandem in the rear part of the fuselage. The baseline technology assumptions adopted for the fuel-cell powerplant are derived by averaging and harmonizing inputs collected within ongoing research projects in which the University of Naples Federico II is involved, dealing with hydrogen-based fuel-cell propulsion for regional aviation applications with a comparable 2040 EIS target.

The main technological assumptions linked to the powerplant have been collected in Table 1. The liquid-hydrogen storage system is modelled assuming cryogenic storage with vacuum and multi-layer insulation. The tanks are sized to provide a dormancy capability of 240 min at ISA+40 °C without venting. The tank gravimetric index is not prescribed as a fixed input, but is calculated during the sizing process, with baseline values of the order of 40%. The fuel-cell system is characterized by a baseline gravimetric and volumetric power density equal to 2.0 kW/kg and 2.0 kW/L, respectively, with a nominal voltage of 800 V. The assumed fuel-cell efficiency varies with the operating condition, with values equal to 53% at maximum power and 63% at minimum power.

The balance-of-plant contributions associated with the fuel-cell system are represented through simplified aircraft-level assumptions. The air supply line and cooling line are associated with dedicated gravimetric power densities, equal to 8.0 kW/kg and 2.5 kW/kg, respectively. The power extraction associated with these systems is assumed to increase with altitude, from 7.2% of the fuel-cell-system power at sea level, ISA conditions, to 20% at 8500 m, ISA conditions. A fraction equal to 9.5% of the heat generated by the fuel-cell system is assumed to be removed through the exhaust. The cooling-line outlet speed recovery is set to 80% in the baseline case. The electric power line includes electric motors, cables, inverters, fuel-cell-system converters, and reduction gearboxes. The adopted component efficiencies are 95% for the electric motor, 99% for the inverter, 99% for the fuel-cell-system converter, 99.5% for the cables, and 99.5% for the reduction gearbox.

Starting from this baseline set of assumptions, six additional technology-variation sets are introduced to quantify the aircraft-level sensitivity to selected fuel-cell-powerplant parameters. Each set modifies one specific technology-related assumption while keeping the remaining assumptions unchanged. The first set increases the fuel-cell efficiency from 53% to 55% at maximum power and from 63% to 65% at minimum power. The second set increases the fuel-cell-system gravimetric power density from 2.0 kW/kg to 2.2 kW/kg. The third set improves the cooling-line gravimetric power density from 2.5 kW/kg to 2.75 kW/kg, while the fourth set improves the air-supply-line gravimetric power density from 8.0 kW/kg to 8.8 kW/kg. The fifth set assumes a 10% increase in the liquid-hydrogen tank gravimetric index. Finally, the sixth set increases the cooling-line outlet speed recovery from 80% to 90%. These variations are intended to isolate the impact of plausible improvements in the main subsystems of the hydrogen fuel-cell powerplant.

For each technology set, including the baseline one, a full-factorial aircraft-level investigation is performed by varying the wing planform area and the nominal electric power of the fuel-cell system. The nominal electric power refers to the gross fuel-cell-system power before the power off-takes associated with the balance of plant. The objective of the parametric study is to generate response surfaces and identify the combination of wing area and installed fuel-cell power that minimizes the design mission energy consumption while satisfying the imposed top-level aircraft requirements.

During this investigation, the wing span is kept fixed and equal to 35.9 m. Consequently, the wing aspect ratio is automatically updated as a function of the selected wing planform area. The horizontal and vertical tail surfaces are also automatically resized in order to preserve constant tail volume coefficients with respect to the baseline aircraft. The fuselage length is updated through the hydrogen-storage integration loop described in the previous section, as a function of the hydrogen mass required for the design mission and of the resulting cryogenic tank size.

Because of the assumed 2040 EIS target, the hydrogen-powered configuration is also assumed to benefit from airframe-level technological improvements with respect to a 2020 state-of-the-art conventional regional turboprop aircraft. A structural mass reduction of approximately 10% is applied

to the main structural components, including wing, fuselage, tails, and nacelles, reflecting the expected use of advanced lightweight composite materials. From an aerodynamic perspective, a 50% reduction of the excrescence and interference contributions to the zero-lift drag coefficient is assumed for all hydrogen-powered configurations.

Table 1 – Baseline and modified technology-level assumptions adopted for the liquid-hydrogen fuel-cell powerplant of the full-electric regional aircraft. Sets 1–6 identify the single-parameter variations considered in the sensitivity study, while unchanged assumptions are indicated by dashes.

Powerplant-related variable	Baseline values	Set 1	Set 2	Set 3	Set 4	Set 5	Set 6
Hydrogen tank							
Tank technology	Cryogenic	-	-	-	-	-	-
Capability	240 min @ISA+40°C w/o venting	-	-	-	-	-	-
Insulation	Vacuum + multi-layer insulation	-	-	-	-	-	-
Number of tanks	2	-	-	-	-	-	-
Gravimetric index	Calculated (≈40%)	-	-	-	-	+10%	-
Fuel cell system (FCS)							
Gravimetric power density	2.0 kW/kg	-	2.2	-	-	-	-
Volumetric power density	2.0 kW/L	-	-	-	-	-	-
Efficiency @max. power	53.0%	55.0%	-	-	-	-	-
Efficiency @min. power	63.0%	65.0%	-	-	-	-	-
Nominal voltage	800 V	-	-	-	-	-	-
FCS air supply line (ASL) and cooling line (CL)							
ASL gravimetric power density	8.0 kW/kg	-	-	-	8.8	-	-
CL gravimetric power density	2.5 kW/kg	-	-	2.75	-	-	-
FCS converter power density	63.0 kW/kg	-	-	-	-	-	-
FCS converter efficiency	99.0%	-	-	-	-	-	-
FCS-generated heat % removed through the exhaust	9.5%	-	-	-	-	-	-
Speed recovery at CL outlet	80%	-	-	-	-	-	90%
ASL+CL FCS power extraction @SL, ISA	7.2%	-	-	-	-	-	-
ASL+CL FCS power extraction @8500 m, ISA	20.0%	-	-	-	-	-	-
Power line (PL)							
Electric motor + cables power density	6.0 kW/kg	-	-	-	-	-	-
Electric motor inverter power density	63.0 kW/kg	-	-	-	-	-	-
Electric motor efficiency	95.0%	-	-	-	-	-	-
Electric motor Inverter efficiency	99.0%	-	-	-	-	-	-
Cables efficiency	99.5%	-	-	-	-	-	-
Reduction gearbox efficiency	99.5%	-	-	-	-	-	-

2.2.2 Battery-based parallel hybrid-electric configuration

The second aircraft-level analysis concerns an 80-passenger regional aircraft with an 800 nm design mission, equipped with a parallel hybrid-electric propulsion system. The aircraft adopts a two-engine layout, in which each propulsive unit combines a conventional thermal branch and a battery-electric branch. The total shaft power available at each engine station is therefore given by the sum of the thermal contribution and the electric contribution. The power-management strategy assumes electric

boost during the most power-demanding flight phases, namely take-off and climb, while an *isopower* strategy is adopted during cruise.

All the key technological assumptions for the hybrid-electric battery-based configurations examined in this study have been collected in Table 2. The baseline battery gravimetric energy density is set to 250 Wh/kg. Two additional, less conservative values are also investigated, equal to 325 Wh/kg and 400 Wh/kg, in order to evaluate the effect of battery technology improvement on aircraft-level performance and fuel-saving potential. The battery system is further characterized by a volumetric energy density of 420 Wh/L, an efficiency of 93%, and a nominal voltage of 800 V. The installed energy content is varied between 200 kWh and 800 kWh per battery pack, meaning that each hybrid-electric engine can be supplied by a battery pack within this capacity range.

The conventional thermal branch is modelled using PW127-like gas-turbine characteristics. Specific fuel consumption, gravimetric power density, and volumetric power density are calculated and scaled using semi-empirical relationships as a function of the selected gas-turbine shaft power. The electric branch includes the electric motor and inverter. The electric motor gravimetric power density is assumed equal to 10.0 kW/kg, while the inverter gravimetric power density is set to 15.0 kW/kg. The corresponding efficiencies are 96% for the electric motor and 98% for the inverter.

For each assumed battery gravimetric energy density, the analysis explores different combinations of total shaft power, hybridization level, and installed battery energy. The total shaft power per engine unit is varied from 2700 kW to 3600 kW, considering four discrete values: 2700, 3000, 3300, and 3600 kW. The hybridization level is varied between 10% and 30%, where this value represents the maximum fraction of the total shaft power that can be supplied by the electric branch. As a result, the electric contribution ranges from 270 kW per engine in the lowest-power, lowest-hybridization case to 1080 kW per engine in the highest-power, highest-hybridization case. The remaining power is supplied by the thermal branch (Table 3).

Contrary to the hydrogen-powered configurations, the battery-based hybrid-electric variants do not include structural or aerodynamic improvements with respect to state-of-the-art regional turboprop aircraft. This assumption is consistent with the shorter-term EIS horizon considered for this architecture. Therefore, the airframe technology level is kept aligned with that of a modern conventional regional aircraft.

The hybrid-electric parametric study is performed at fixed aircraft geometry. The wing planform area is set to 80 m^2 and the wing aspect ratio is set to 15. These values are selected because they allow an equivalent conventional reference aircraft to satisfy the same set of TLARs adopted for the hybrid-electric study. For each combination of battery energy density, installed battery capacity, hybridization level, and total shaft power, JPAD evaluates the resulting mass breakdown, fuel consumption, battery energy usage, and compliance with ground, climb, and cruise performance requirements.

Table 2 – Technology-level assumptions adopted for the battery-based parallel hybrid-electric aircraft, including battery-pack characteristics, electric propulsion-chain efficiencies, thermal-engine modelling assumptions, and the parametric ranges explored in terms of battery capacity and gravimetric energy density.

Powerplant-related variable	Baseline values	Set 1	Set 2
Battery system			
Gravimetric energy density	250 Wh/kg	325	400
Volumetric energy density	420 Wh/L	-	-
Efficiency	93.0%	-	-
Energy content	200 – 800 kWh	-	-
Nominal voltage	800 V	-	-
Gas turbine engine			
Specific fuel consumption	PW127-like[1]	-	-
Gravimetric power density	PW127-like[1]	-	-
Volumetric power density	PW127-like[1]	-	-

Electric motor			
Gravimetric power density	10.0 kW/kg	-	-
Efficiency	96.0%	-	-
Inverter gravimetric power density	15.0 kW/kg	-	-
Inverter efficiency	98.0%	-	-

[1] Calculated and scaled using semi-empirical relationships as a function of the selected actual gas-turbine shaft power.

Table 3 – Power-split matrix adopted for the battery-based parallel hybrid-electric configurations. For each total shaft power per engine unit and hybridization factor, the table reports the corresponding electric and thermal shaft-power contributions considered in the aircraft-level analyses.

		Hybridization factor		
Shaft power		**10%**	**20%**	**30%**
2,700 kW	Electric contribution	270 kW	540 kW	810 kW
	Thermal contribution	2,430 kW	2,160 kW	1,890 kW
3,000 kW	Electric contribution	300 kW	600 kW	900 kW
	Thermal contribution	2,700 kW	2,400 kW	2,100 kW
3,300 kW	Electric contribution	330 kW	660 kW	990 kW
	Thermal contribution	2,970 kW	2,640 kW	2,310 kW
3,600 kW	Electric contribution	360 kW	720 kW	1,080 kW
	Thermal contribution	3,240 kW	2,880 kW	2,520 kW

2.3 Definition of top-level aircraft requirements

The two aircraft-level investigations are carried out with reference to two separate sets of TLARs, summarized in Table 4. The requirements are selected to represent regional propeller-driven aircraft applications. In both cases, the requirements are used as sizing and feasibility constraints within the JPAD-based design workflow, so that each candidate configuration is assessed not only in terms of mission energy or fuel consumption, but also in terms of compliance with prescribed operational capabilities.

The hydrogen fuel-cell aircraft is sized for a 1,000 nm design range and a design payload of 100 passengers, assuming a passenger mass of 95 kg. The aircraft is required to reach an initial cruise altitude of 22,000 ft and to operate at a cruise Mach number of 0.53. Ground performance constraints are imposed through maximum take-off and landing field lengths equal to 1,500 m. The aircraft is also required to satisfy Approach Category C and ICAO airport code C compatibility.

The battery-based parallel hybrid-electric aircraft is instead defined around an 80-passenger mission with a design range of 800 nm, again assuming 95 kg per passenger. The required initial cruise altitude is 20,000 ft, while the cruise Mach number is set to 0.45. More demanding ground-performance requirements are adopted for this case, with both take-off and landing field lengths limited to 1,300 m. The aircraft is required to comply with Approach Category B and ICAO airport code C.

Table 4 – Top-level aircraft requirements adopted for the hydrogen fuel-cell and battery-based hybrid-electric regional aircraft studies.

	Sets of requirements	
Requirements	**Fuel-cell aircraft**	**Hybrid battery aircraft**
Design range	1,000 nm	800 nm
Design payload	100 PAX @95 kg	80 PAX @95 kg
Initial cruise altitude capability	22,000 ft	20,000 ft
Cruise Mach number	0.53	0.45

Take-off field length (TOFL)	1,500	1,300
Landing field length (LFL)	1,500	1,300
Approach category *	C	B
ICAO airport code **	C	C
Reserves	100-nm alternate, 30-min holding, 5% contingency fuel	
LH2 tank dormancy requirement ***	240 min @ ISA+40°C w/o venting	-

* B (91 < approach CAS < 120 kn), C (121 < approach CAS < 140 kn).

** C (24 < wing span < 36).

*** Only applicable to fuel-cell aircraft.

3. Results and discussion

3.1 *Hydrogen fuel-cell full-electric configuration*

The first set of results concerns the full-electric liquid-hydrogen fuel-cell aircraft. For each fuel-cell technology set introduced in Subsection 2.2.1, the aircraft was optimized by varying the wing planform area and the nominal electric power of each fuel-cell system. The optimization objective was the minimization of the hydrogen consumption on the 1,000 nm design mission, while satisfying the complete set of top-level aircraft requirements of Table 4. The fuel-cell power reported in the following refers to the nominal gross electric power of each fuel-cell system, before the power off-takes associated with the fuel-cell balance of plant.

Figure 2 shows the design space obtained for the baseline technology assumptions. The feasible domain is represented in the wing planform area - fuel-cell power plane, together with the main performance constraints and the block hydrogen consumption contours. The selected optimum is located on the boundary of the feasible region. In particular, the take-off field length (TOFL) requirement drives the minimum acceptable wing area, while the initial cruise altitude capability drives the minimum installed fuel-cell power. As a result, the optimum is found close to the intersection of these two active constraints. The same behaviour is observed for all the alternative technology sets: the TOFL and ceiling-related constraints remain the main drivers of the optimum selection, while the landing field length (LFL), approach speed, and maximum cruise Mach number constraints do not directly determine the optimum point.

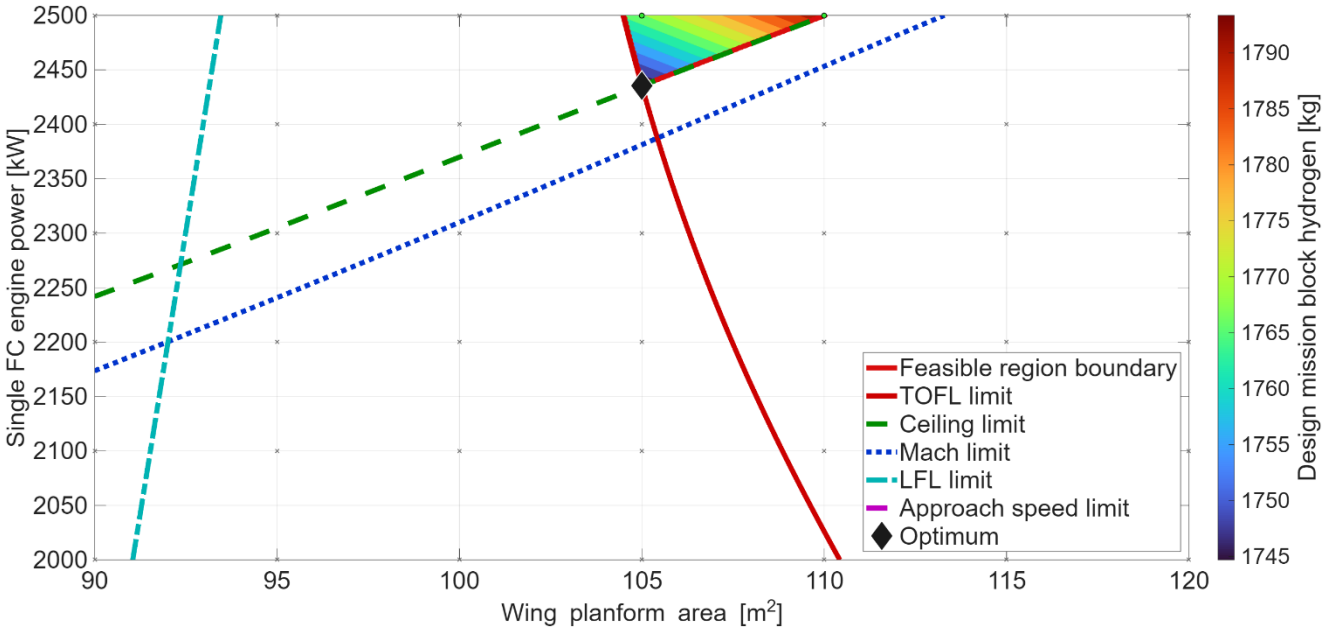


Figure 2 – Design mission block hydrogen contour and design space constraints for the set of requirements specific to hydrogen-powered aircraft listed in Table 4.

For the baseline case, the optimized configuration is obtained with a wing planform area of 105.0 m^2 and a nominal fuel-cell power of 2,435 kW per propulsive unit. Since the wing span is kept fixed at 35.9 m, this corresponds to an aspect ratio of about 12.3. The resulting aircraft has a maximum take-off mass (MTOM) of 48.8 t, an operating empty mass (OEM) of 37.2 t, and a total powerplant mass of 16.8 t. The sizing hydrogen mass (i.e., the total mass of hydrogen, including diversion and additional reserves) is 2,284 kg, while the hydrogen consumed on the 1,000 nm design mission is 1,744 kg. The final fuselage length is 38.6 m, as obtained from the liquid-hydrogen tank integration loop.

The comparison among the optimized configurations highlights the different aircraft-level relevance of the examined technology parameters. Table 5 summarizes some of the main optimized aircraft characteristics obtained for the baseline case and for the six alternative fuel-cell technology sets, while Figure 3 reports the corresponding percentage variations with respect to the baseline for selected aircraft-level quantities. The largest improvement is obtained for Set 6, in which the fuel-cell cooling-line outlet speed recovery is increased. This assumption directly reduces the drag penalty associated with the cooling installation: the cruise zero-lift drag coefficient decreases from 373.7 to 310.7 drag counts, while the maximum cruise aerodynamic efficiency increases from 14.9 to 16.3. As a consequence, the required installed fuel-cell power decreases to 2,098 kW per propulsive unit, and the 1,000 nm design mission hydrogen consumption is reduced to 1,493 kg, corresponding to a 14.4% reduction with respect to the baseline. The lower mission energy demand also leads to a lower sizing hydrogen mass, a shorter fuselage, and a reduced aircraft mass. The maximum take-off mass decreases to 45.6 t, while the operating empty mass is reduced to 34.3 t, also as a consequence of the lower nominal fuel-cell power required and the corresponding reduction in powerplant mass.

The second most relevant improvement is obtained for Set 1, which assumes higher fuel-cell efficiency. In this case, the reduction in hydrogen consumption is linked both to the improved energy conversion efficiency and to the lower heat rejection requirement. The optimized wing area decreases to 102.5 m^2, while the fuel-cell power decreases to 2,307 kW per unit. The 1,000 nm mission hydrogen consumption is reduced from 1,744 kg to 1,592 kg, corresponding to an 8.8% improvement. The MTOM decreases by about 3.6%, while the powerplant mass decreases by about 7.2%. The cruise zero-lift drag coefficient is also reduced, mainly because the lower heat rejection requirement leads to a smaller cooling-related drag contribution.

The effect of improving the liquid-hydrogen tank gravimetric index is represented by Set 5. This case mainly affects the aircraft through a reduction of the hydrogen storage-system mass. The tank mass decreases from 4,503 kg in the baseline case to 3,815 kg, corresponding to a reduction of about 15%. This leads to a lower MTOM and to a smaller optimum wing area and fuel-cell power. However, since the improvement does not directly affect the fuel-cell conversion efficiency or the cooling drag penalty, the reduction in design mission hydrogen consumption is more limited, equal to about 2.9% with respect to the baseline.

The remaining technology variations have a more moderate impact on the optimized aircraft. Increasing the fuel-cell-system gravimetric power density, as considered in Set 2, reduces the powerplant mass and leads to a 2.1% reduction in design mission hydrogen consumption. Improving the cooling-line gravimetric power density, as considered in Set 3, provides a 1.5% reduction. The improvement of the air-supply-line gravimetric power density in Set 4 has the smallest effect, with a block hydrogen reduction of about 0.5%. These results are consistent with the relative contribution of the different subsystems to the powerplant mass and with the fact that these sets mainly affect mass, without significantly modifying the propulsion-chain efficiency or the aerodynamic penalties.

The powerplant mass breakdown further helps to correctly interpret these trends. In the baseline configuration, the fuel-cell stacks account for approximately 52% of the combined fuel-cell and auxiliary-system mass, while the cooling line contributes about 33% and the air supply line about 13%. The remaining contribution is associated with power electronics. In addition, the hydrogen tank system, including tank auxiliary systems and crash structure, accounts for approximately one quarter of the total powerplant-related mass.

The comparison among the different technology sets should be interpreted within the scope and

assumptions of the present study. In particular, the variations applied to fuel-cell efficiency, fuel-cell gravimetric power density, fuel-cell balance-of-plant mass, liquid-hydrogen tank gravimetric index, and fuel-cell cooling-related aerodynamic penalty are treated independently, in order to isolate their aircraft-level effects. In practice, some of these quantities may be coupled. For example, fuel-cell efficiency and stack power density are not fully independent, since changes in operating point, current density, and system design may affect both the specific power and the amount of heat to be rejected. Therefore, the results should not be interpreted as a definitive ranking of technology priorities, but rather as an indication of the relative sensitivities obtained for the selected 100-passenger, high-wing, four-engine, propeller-driven hydrogen aircraft and for the adopted set of TLARs.

Within this design space, the most influential variations are those that modify either the mission energy conversion efficiency or the aerodynamic penalty associated with the fuel-cell installation, because they affect not only hydrogen consumption but also the converged aircraft mass, required installed power, and storage-system sizing. Conversely, isolated improvements in subsystem gravimetric power density mainly act through mass reduction and produce more limited changes in the optimized configuration.

Table 5 – Optimized aircraft characteristics obtained for the baseline fuel-cell technology assumptions and for the six alternative technology sets. The reported LH2 tank mass includes the tank structure, insulation, auxiliary storage-system components, and crash structure mass. The powerplant mass includes the fuel-cell systems, fuel-cell ancillary components, electric power-line components, propellers, and LH2 storage system.

Case	Wing area [m^2]	FCS power per unit [kW]	MTOM [kg]	OEM [kg]	LH2 tank mass [kg]	Powerplant mass [kg]	1,000-nm mission block fuel [kg]	250-nm mission block fuel [kg]
Baseline	*105.0*	*2,435*	*48,785*	*37,223*	*4,503*	*16,841*	*1,744.4*	*430.4*
Set 1	102.5	2,307	47,009	35,629	4,186	15,627	1,591.7	392.8
Set 2	103.0	2,383	47,806	36,288	4,426	16,059	1,707.7	421.4
Set 3	103.5	2,399	48,128	36,597	4,450	16,320	1,718.9	424.1
Set 4	104.5	2,422	48,538	36,987	4,484	16,644	1,735.2	428.2
Set 5	102.2	2,364	47,448	35,946	3,815	15,780	1,694.1	418.1
Set 6	106.1	2,098	45,558	34,294	3,981	14,555	1,493.1	367.8

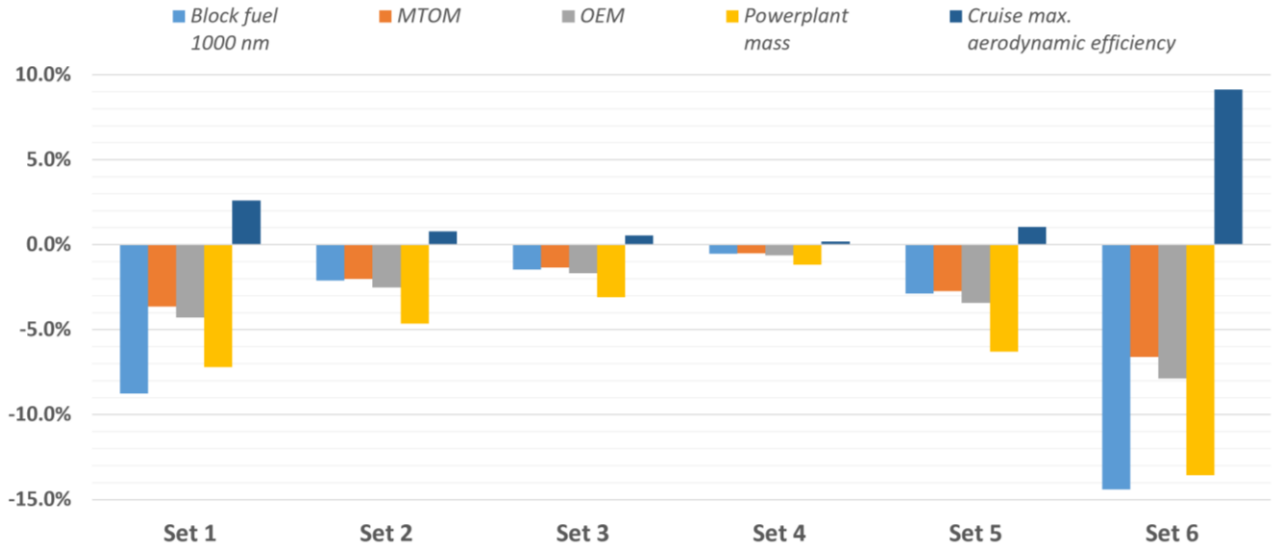


Figure 3 – Percentage variation of selected optimized aircraft characteristics with respect to the baseline fuel-cell technology case. Variations are reported for the six alternative technology sets and refer to the corresponding optimized configurations satisfying the imposed TLARs.

3.2 *Battery-based parallel hybrid-electric configuration*

The second part of the results concerns the battery-based parallel hybrid-electric aircraft introduced in Subsection 2.2.2. Differently from the hydrogen fuel-cell case, the aircraft geometry is kept fixed during this analysis, with a wing planform area of 80 m^2 and a wing aspect ratio equal to 15. This wing area is larger than that of the conventional reference aircraft considered for comparison, for which a wing planform area of about 70 m^2 was sufficient to satisfy the TLARs of Table 4. The increase to 80 m^2 was introduced for the hybrid-electric baseline in order to provide additional margin with respect to landing field length and approach speed requirements, considering the expected mass increase associated with the integration of the battery-electric branch. The parametric investigation is therefore focused on the effect of propulsion-system parameters, namely battery gravimetric energy density, installed battery energy, hybridization factor, and total shaft power per engine unit. The results are compared with a fully conventional reference aircraft, also modelled in JPAD and sized to satisfy the same TLARs listed in Table 4. The reference aircraft has a wing aspect ratio equal to 15 and two gas-turbine engines providing approximately 2735 kW each. Its 800 nm design mission block fuel is equal to 2,327 kg, with an MTOM of about 27.8 t and an OEW of about 17.25 t.

Figure 4a and Figure 4b show two representative subsets of the hybrid-electric parametric study. Both figures refer to a fixed total shaft power of 3,000 kW per engine unit and report the relationship between 800 nm block fuel and MTOM for different battery energy contents and battery gravimetric energy densities. Figure 4a refers to a hybridization factor of 10%, while Figure 4b refers to a hybridization factor of 20%. In both cases, the curves clearly show the trade-off introduced by the battery-electric branch: increasing the installed battery energy reduces the mission block fuel, but it also increases the aircraft mass. A larger battery allows a greater use of electric power during the mission, but also introduces a mass penalty that affects the converged MTOM.

For the 10% hybridization case, the fuel-saving potential remains relatively limited. With the most conservative battery assumption of 250 Wh/kg, the block fuel decreases from 2,346.5 kg to 2,284.1 kg when the single-battery energy content increases from 360.7 kWh to 721.4 kWh. This corresponds to a variation from a slight fuel penalty of about 0.8% to a fuel saving of about 1.8% with respect to the conventional reference aircraft. Higher battery gravimetric energy densities improve the trade-off. For 325 Wh/kg, the block fuel ranges from 2,329.4 kg to 2,237.8 kg, while for 400 Wh/kg it ranges from 2,315.9 kg to 2,211.7 kg. In the latter case, the maximum fuel saving reaches approximately 5.0% with respect to the conventional reference. However, this improvement is obtained at the expense of a substantial MTOM increase: even for the most favourable 400 Wh/kg assumption, the MTOM varies between about 30.6 t and 32.5 t, remaining significantly higher than the 27.8 t of the conventional reference.

Increasing the hybridization factor to 20% produces a more evident reduction in block fuel. For the 250 Wh/kg battery assumption, the block fuel varies between 2,250.7 kg and 2,224.4 kg, corresponding to a reduction of about 3.3–4.4% with respect to the conventional aircraft. With 325 Wh/kg, the reduction becomes more significant, with block fuel values between 2,226.8 kg and 2,162.2 kg. The most favourable trend is obtained for 400 Wh/kg, for which the block fuel decreases from 2,215.5 kg to 2,128.9 kg as the single-battery energy content increases from 360.7 kWh to 721.4 kWh. This corresponds to a maximum fuel saving of about 8.5% relative to the conventional reference. Nevertheless, the associated mass penalty remains substantial, with MTOM values ranging from about 30.6 t to 32.5 t for the 400 Wh/kg case and increasing up to more than 35 t for the 250 Wh/kg, high-capacity case.

The comparison between the 10% and 20% hybridization cases shows that a higher electric power share can provide larger mission fuel reductions, especially when coupled with higher battery gravimetric energy density. However, the benefits are not governed by hybridization factor alone. At fixed total shaft power, the effective advantage depends on the balance among thermal-engine downsizing, electric-machine sizing, installed battery mass, available battery energy, and the amount of electric boost that can be usefully exploited during the mission. For this reason, increasing the battery capacity does not lead to proportional reductions in block fuel. This effect is particularly evident at low battery gravimetric energy density and higher hybridization factor. For instance, in the 20% hybridization case with 250 Wh/kg batteries, increasing the single-battery energy content from 360.7 kWh to 721.4 kWh causes a substantial MTOM increase, while the block fuel reduction remains limited to about 26 kg over the whole range. In this condition, the additional battery energy is partly offset by the battery mass penalty, leading to a progressive flattening of the fuel curve.

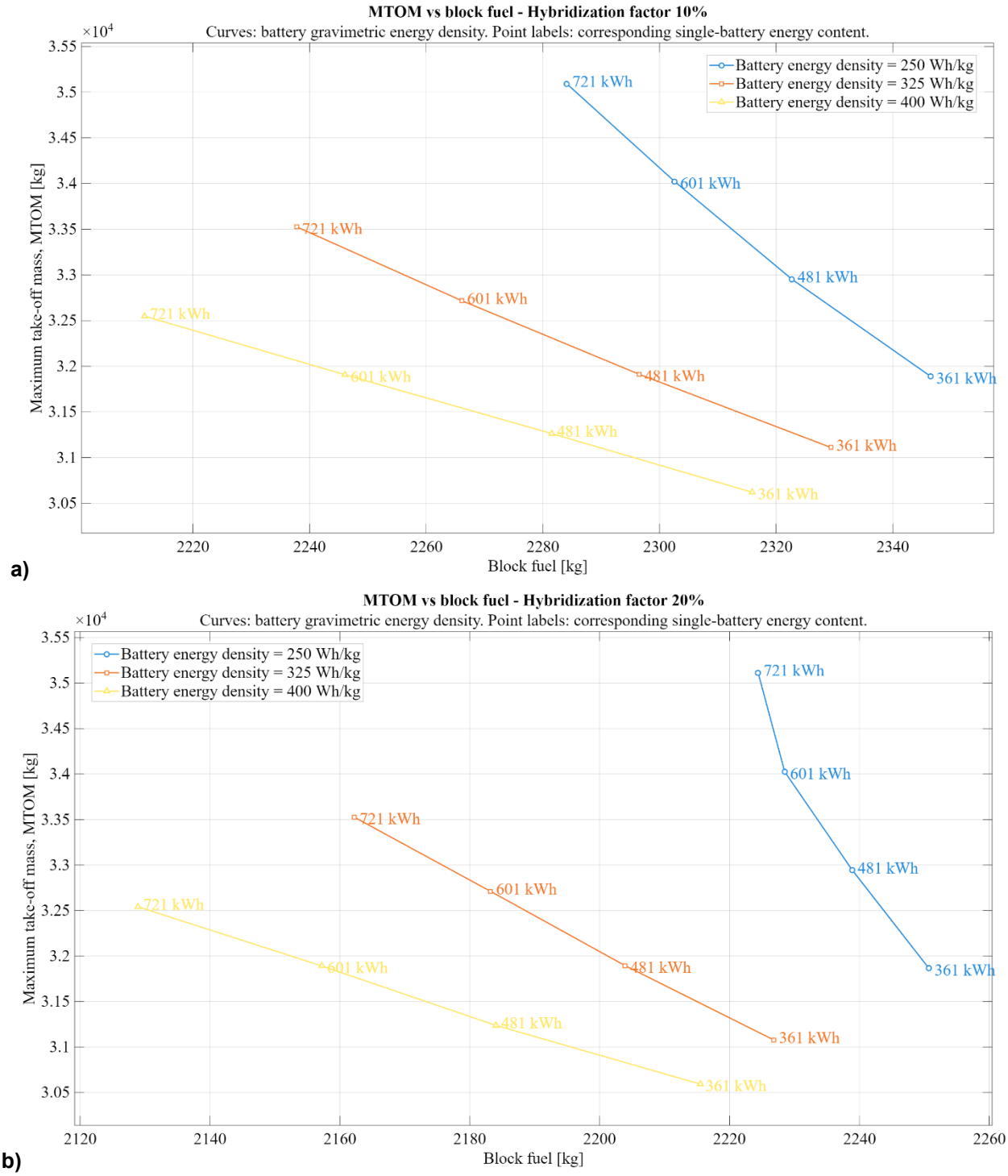


Figure 4 – Effect of battery energy content and battery gravimetric energy density on MTOM and 800 nm block fuel for the battery-based parallel hybrid-electric aircraft at fixed total shaft power equal to 3,000 kW per engine unit: a) hybridization factor 10%; b) hybridization factor 20%. Point labels indicate the energy content of each battery pack.

The trends shown in Figure 4a and Figure 4b provide useful insight into the isolated effect of battery capacity, battery gravimetric energy density, and hybridization factor on block fuel and MTOM. However, these figures do not account for the complete constraint-based selection of feasible configurations. For this reason, the final step of the analysis consists of identifying, for each battery gravimetric energy density, the combination of total shaft power per engine, hybridization factor, and single-battery energy content that minimizes the 800 nm design mission block fuel while satisfying the TLARs of Table 4. The resulting optima are summarized in Table 6.

When the original set of TLARs is retained, including a target cruise Mach number equal to 0.45, the optimized solutions show that the integration of the hybrid-electric powerplant does not provide a

meaningful fuel-saving advantage over the conventional reference aircraft within the explored design space. For battery gravimetric energy densities between 250 Wh/kg and 375 Wh/kg, the optimized block fuel remains higher than that of the conventional aircraft, with penalties ranging from about 2.9% at 250 Wh/kg to about 0.4% at 375 Wh/kg. Only the 400 Wh/kg case reaches a value slightly below the reference, with a block fuel of 2,323.2 kg, corresponding to a very small reduction of about 0.15%.

The optimized configurations obtained for the original TLAR set also require relatively high installed shaft power, between about 3185 kW and 3256 kW per engine, despite the conventional reference aircraft requiring about 2735 kW per engine. This increase is mainly driven by the need to recover the performance penalties associated with the higher aircraft mass and the fixed hybrid-electric airframe geometry. The optimized hybridization factors remain close to the lower part of the investigated range, varying from 10% for the lowest battery energy density cases to about 11.7% for the 400 Wh/kg case. The corresponding single-battery energy content increases from about 240 kWh at 250 Wh/kg to about 445 kWh at 400 Wh/kg. The resulting MTOM remains significantly higher than that of the conventional reference aircraft, with values around 31.0–31.5 t compared with about 27.8 t.

These results help to qualify the fuel-saving trends previously observed in Figure 4a and Figure 4b. In particular, some configurations at fixed 3,000 kW per engine and higher hybridization factor showed more attractive block-fuel reductions, especially for high battery gravimetric energy density and large battery capacity. However, once all TLARs are imposed simultaneously, the feasible optima move toward a more conservative combination of hybridization factor and battery energy. Therefore, the apparent fuel-saving potential shown by the unconstrained parametric trends is substantially reduced when ground performance, climb capability, cruise Mach number, and approach constraints are considered together.

A second optimization was then performed by slightly relaxing the cruise Mach requirement from 0.45 to 0.43, while keeping the remaining TLARs unchanged. This modification already improves the attractiveness of the hybrid-electric solutions. At 250 Wh/kg, the optimized block fuel is essentially equal to the conventional reference, while increasing battery gravimetric energy density progressively leads to fuel savings. The block fuel decreases from 2,326.8 kg at 250 Wh/kg to 2,261.5 kg at 400 Wh/kg, corresponding to a maximum reduction of about 2.8% with respect to the conventional aircraft. The optimized shaft power is also reduced with respect to the original Mach 0.45 case, with values between about 2,915 kW and 3,152 kW per engine. The hybridization factor increases moderately, reaching values around 15–16% for the highest battery energy density cases. This indicates that a limited relaxation of the cruise-speed requirement allows the electric branch to provide a more effective contribution.

A further reduction of the cruise Mach requirement to 0.41 leads to more noticeable block-fuel reductions. In this case, the optimized shaft power decreases to the lower bound of the investigated range, equal to 2,700 kW per engine for most battery energy density assumptions. The block fuel decreases from 2,262.6 kg at 250 Wh/kg to 2,192.2 kg at 400 Wh/kg. This corresponds to fuel savings ranging from about 2.8% to about 5.8% with respect to the conventional reference aircraft. The optimized hybridization factors remain close to 10–11%, while the single-battery energy content increases with battery gravimetric energy density, from about 270 kWh to about 448 kWh. The MTOM remains around 30.5–30.8 t, still higher than the conventional reference, but lower than several of the configurations obtained for the higher Mach requirements.

Overall, the three optimization sets show that the fuel-saving potential of the battery-based parallel hybrid-electric architecture is strongly constrained by the selected TLARs. Under the original cruise Mach requirement of 0.45, the additional mass associated with the battery-electric branch offsets most of the benefit provided by partial electrification. The advantage becomes more evident only when the cruise Mach requirement is relaxed, because the required installed power and the aircraft-level penalties associated with the hybrid-electric installation are reduced. Therefore, for the considered 800 nm regional mission and for the explored battery technology assumptions, hybrid-electric propulsion appears more attractive when combined with less demanding cruise-speed requirements.

Table 6 - Optimized TLAR-compliant hybrid-electric configurations for different battery gravimetric energy densities and cruise Mach requirements. For each battery technology level, the table reports the optimized total shaft power per engine, hybridization factor, single-battery energy content, 800-nm design mission block fuel, percentage variation with respect to the conventional reference aircraft, and MTOM.

Optimized configurations satisfying the baseline TLARs						
Battery gravimetric energy density [Wh/kg]	**Shaft power per engine [kW]**	**Hybridization factor**	**Battery energy content per pack [kWh]**	**800-nm design mission block fuel [kg]**	**Δ% Block fuel relative to reference**	**MTOM [kg]**
250	3,185.1	10.0%	240.5	2,393.6	2.88%	30,991
275	3,202.5	10.0%	309.6	2,384.1	2.47%	31,417
300	3,199.9	10.0%	336.2	2,372.2	1.96%	31,393
325	3,256.2	11.5%	374.2	2,358.5	1.37%	31,471
350	3,255.2	11.5%	396.9	2,347.8	0.91%	31,443
375	3,253.1	11.6%	419.7	2,336.1	0.41%	31,394
400	3,250.4	11.7%	444.9	2,323.2	-0.15%	31,337

Optimized configurations satisfying the TLARs with cruise Mach target reduced to 0.43						
Battery gravimetric energy density [Wh/kg]	**Shaft power per engine [kW]**	**Hybridization factor**	**Battery energy content per pack [kWh]**	**800-nm design mission block fuel [kg]**	**Δ% Block fuel relative to reference**	**MTOM [kg]**
250	2,915.5	10.0%	240.5	2,326.8	0.01%	30,663
275	2,931.5	10.0%	286.9	2,319.3	-0.31%	30,909
300	3,029.9	12.6%	322.2	2,310.4	-0.70%	31,089
325	3,152.0	15.9%	355.1	2,298.1	-1.22%	31,217
350	3,136.0	15.5%	385.7	2,287.9	-1.66%	31,232
375	3,139.1	15.4%	426.0	2,274.5	-2.24%	31,297
400	3,135.5	15.5%	450.4	2,261.5	-2.80%	31,231

Optimized configurations satisfying the TLARs with cruise Mach target reduced to 0.41						
Battery gravimetric energy density [Wh/kg]	**Shaft power per engine [kW]**	**Hybridization factor**	**Battery energy content per pack [kWh]**	**800-nm design mission block fuel [kg]**	**Δ% Block fuel relative to reference**	**MTOM [kg]**
250	2,700.0	10.5%	270.4	2,262.6	-2.75%	30,686
275	2,700.0	10.5%	290.1	2,253.6	-3.14%	30,668
300	2,700.0	10.6%	313.2	2,242.0	-3.64%	30,641
325	2,700.0	10.8%	340.3	2,227.1	-4.28%	30,601
350	2,700.0	10.8%	357.5	2,218.8	-4.63%	30,555
375	2,700.0	10.7%	382.4	2,209.0	-5.05%	30,539
400	2,740.1	11.4%	447.7	2,192.2	-5.78%	30,762

These results also highlight some limitations of the present analysis. First, the adopted power-management strategy for cruise is based on an isopower logic, rather than on a boost strategy. This means that, during cruise, the hybrid-electric powerplant is not necessarily exploited to maximize the available shaft power, but rather to redistribute the required power between the thermal and electric branches. For configurations characterized by particularly high aircraft mass, this assumption may limit the effective cruise performance benefit of the electric branch and may penalize the ability of the aircraft to satisfy the cruise-related requirements. Alternative cruise strategies, including limited electric boost, could therefore lead to different feasible regions and should be investigated in future developments.

Second, the comparison with the conventional reference aircraft is performed on the 800 nm design mission. A shorter typical mission would probably be more representative of many regional

operations and could better exploit the potential of battery-assisted propulsion. However, such a comparison was not retained here because, for several combinations of hybridization factor and installed battery energy, the batteries were not fully discharged on the shorter 250 nm mission considered as a possible reference. This would make the comparison among configurations less consistent, since different cases would use different fractions of the installed battery energy.

Finally, the hybrid-electric study is performed at fixed aircraft geometry, with the wing planform area set to 80 m^2 and the aspect ratio set to 15. The optimization is therefore limited to propulsion-related variables, namely total shaft power, hybridization factor, and battery energy content. A more complete aircraft-level optimization should also include wing planform area, and possibly other airframe variables, in the same way as performed for the conventional reference. Such an extended design-space exploration could identify more favourable combinations.

4. Conclusions

This paper investigated the aircraft-level impact of technology-related assumptions for advanced regional aircraft equipped with electric and hybrid-electric powertrains. Two case studies were analysed using the JPAD conceptual design framework: a full-electric liquid-hydrogen fuel-cell aircraft and a battery-based parallel hybrid-electric aircraft coupled with gas-turbine engines.

For the hydrogen fuel-cell configuration, the results showed that the optimum design is mainly driven by take-off field length and initial cruise altitude requirements, which determine the required wing area and installed fuel-cell power. Among the examined technology variations, the largest benefit was obtained by improving the cooling-line outlet speed recovery, leading to a 14.4% reduction in 1,000 nm mission hydrogen consumption with respect to the baseline. Increasing fuel-cell efficiency provided the second largest improvement, with an 8.8% reduction. Variations mainly affecting subsystem gravimetric power density produced more limited benefits.

For the battery-based hybrid-electric configuration, the preliminary parametric results showed that increasing battery capacity and hybridization factor can reduce block fuel, but at the cost of a significant MTOM increase. Once the complete set of TLARs was imposed, the achievable fuel-saving potential became more limited. With the original cruise Mach requirement of 0.45, no configuration within the explored design space provided a meaningful block-fuel reduction while satisfying all constraints. Moderate benefits appeared only when the cruise Mach requirement was relaxed.

Overall, the study confirms that the potential of emerging electric propulsion technologies must be assessed at aircraft level, since component-level improvements interact with mass growth, aerodynamic penalties, installed power, energy storage integration, mission requirements, and TLAR compliance. Future work will focus on coupled technology variations for fuel-cell systems, improved modelling of cooling and installation effects, alternative hybrid-electric power-management strategies, and broader aircraft-level optimizations including wing planform variables and shorter typical missions.

5. Contact Author Email Address

mailto: fabrnico@unina.it

6. Copyright Statement

The authors confirm that they, and/or their company or organization, hold copyright on all of the original material included in this paper. The authors also confirm that they have obtained permission, from the copyright holder of any third party material included in this paper, to publish it as part of their paper. The authors confirm that they give permission, or have obtained permission from the copyright holder of this paper, for the publication and distribution of this paper as part of the ICAS proceedings or as individual off-prints from the proceedings.

References

[1] Marciello V, Ruocco M, Nicolosi F, and Di Stasio M. Market analysis, TLARs selection and preliminary design investigations for a regional hybrid-electric aircraft. *Proc 33rd Congress of the International Council of the Aeronautical Sciences (ICAS)*, Stockholm, Sweden, 4-9 September, 2022.

[2] Airbus. *ZEROe: our hydrogen-powered aircraft*. Airbus, available at: https://www.airbus.com/en/innovation/energy-transition/hydrogen/zeroe-our-hydrogen-powered-aircraft (accessed 25/05/2026).

[3] Aerospace Technology Institute (ATI). *FlyZero: Zero-Carbon Emission Aircraft Concepts*. Technical Report FZO-AIN-REP-0007, Aerospace Technology Institute, 2022, available at: https://www.ati.org.uk/wp-content/uploads/2022/03/FZO-AIN-REP-0007-FlyZero-Zero-Carbon-Emission-Aircraft-Concepts.pdf (accessed 25/05/2026).

[4] Rischmüller U, Lessis A, Egerer P, and Hornung M. Conceptual design of a hydrogen-hybrid dual-fuel regional aircraft retrofit. *Aerospace*, Vol. 11, No. 2, 2024.

[5] Palladino V, Bartoli N, Pommier-Budinger V, Benard E, Schmollgruber P, and Jordan A. Optimization of a hydrogen-based hybrid propulsion system under aircraft performance constraints. *Chinese Journal of Aeronautics*, Vol. 36, No. 5, pp 41-56, 2023.

[6] Aliberti P, Simone C, Addesso P, De Piano G, Donsi F, Galdi A, Maritato L, Pantani R, Pianese C, Polverino P, Postiglione F, and Sorrentino M. Fuel cells in aviation: challenges to power the future of flight. *Energy Conversion and Management: X*, Vol. 29, 2026.

[7] Svensson C, Oliveira A and Grönstedt T. Hydrogen fuel cell aircraft for the Nordic market. *International Journal of Hydrogen Energy*, Vol. 61, pp 650-663, 2024.

[8] Ahluwalia R, Wang X, Shah A, Lauer M and Ansell P. Fuel cells for single-aisle regional aircraft: system configuration, performance and cost. *International Journal of Hydrogen Energy*, Vol. 159, 2025.

[9] Palaia G, Abu Salem K, and Quarta AA. Parametric analysis for hybrid–electric regional aircraft conceptual design and development. *Applied Sciences*, Vol. 13, No. 19, 2023.

[10] Spinelli A, Krupa GP, Kipouros T, Laskaridis P, and Berseneff B. Battery pack technological considerations for hybrid-electric regional aircraft feasibility. *The Aeronautical Journal*, Vol. 129, No. 1335, pp 1142-1166, 2025.

[11] Trifari V, Ruocco M, Cusati V, Nicolosi F, and De Marco A. Multi-disciplinary analysis and optimization Java tool for aircraft design. *Proc 31st Congress of the International Council of the Aeronautical Sciences (ICAS 2018)*, Belo Horizonte, Brazil, 9-14 September, 2018.

[12] De Marco A, Di Stasio M, Della Vecchia P, Trifari V, and Nicolosi F. Automatic modeling of aircraft external geometries for preliminary design workflows. *Aerospace Science and Technology*, Vol. 8, 2020.

[13] De Marco A, Trifari V, Nicolosi F and Ruocco M. A simulation-based performance analysis tool for aircraft design workflows. *Aerospace*, Vol. 7, No. 11, 2020.

[14] Prajwal P, Ciampa PD, Della Vecchia P, Ciliberti D, Voskuij M, Charbonnier D, Jungo A, Zhang M, Fioriti M, Anisimov K, and Mirzoyan A. Model based collaborative design & optimization of blended wing body aircraft configuration: AGILE EU project. *Proc 2018 Aviation Technology, Integration, and Operations Conference*, Atlanta, Georgia, 25-29 June, 2018.

[15] Bussemaker JH, Ciampa PD, Singh J, Fioriti M, Cabaleiro C, Wang Z, Peeters DMJ, Hansmann P, Della Vecchia P, and Mandorino M. Collaborative design of a business jet family using the AGILE 4.0 MBSE environment. *Proc 2022 AIAA AVIATION Forum*, Chicago, Illinois, 27 June – 1 July, 2022.

[16] Fioriti M, Cabaleiro C, Lefebvre T, Della Vecchia P, Mandorino M, Liscouet-Hanke S, Jeyaraj A, Donelli G, and Jungo A. Multidisciplinary design of a more electric regional aircraft including certification constraints. *Proc 2022 AIAA AVIATION Forum*, Chicago, Illinois, 27 June – 1 July, 2022.

[17] Winnefeld C, Kadyk T, Bensmann B, Krewer U, and Hanke-Rauschenbach R. Modelling and designing cryogenic hydrogen tanks for future aircraft applications. *Energies*, Vol. 11, No. 1, 2018.

[18] Nicolosi F, Melone G, and Di Stasio M. Impact of thermal management system design on aircraft performance in hydrogen fuel cell powertrains. *Proc AIAA SciTech Forum 2026*, Orlando, Florida, 12-16 January, 2026.